Research Article Vol. 56, No. 16 / June 1 2017 / Applied Optics 4785

applied optics

Hyperspectral remote sensing image retrieval system using spectral and texture features

Jing Zhang,[1,*] Wenhao Geng,[1] Xi Liang,[1] Jiafeng Li,[1] Li Zhuo,[1,2] and Qianlan Zhou[1]

[1]Signal and Information Processing Laboratory, Beijing University of Technology, Beijing 100124, China
[2]Collaborative Innovation Center of Electric Vehicles in Beijing, Beijing 100124, China
*Corresponding author: zhj@bjut.edu.cn

Received 15 February 2017; revised 19 April 2017; accepted 7 May 2017; posted 8 May 2017 (Doc. ID 286672); published 31 May 2017

Although many content-based image retrieval systems have been developed, few studies have focused on hyperspectral remote sensing images. In this paper, a hyperspectral remote sensing image retrieval system based on spectral and texture features is proposed. The main contributions are fourfold: (1) considering the "mixed pixel" in the hyperspectral image, endmembers as spectral features are extracted by an improved automatic pixel purity index algorithm, then the texture features are extracted with the gray level co-occurrence matrix; (2) similarity measurement is designed for the hyperspectral remote sensing image retrieval system, in which the similarity of spectral features is measured with the spectral information divergence and spectral angle match mixed measurement and in which the similarity of textural features is measured with Euclidean distance; (3) considering the limited ability of the human visual system, the retrieval results are returned after synthesizing true color images based on the hyperspectral image characteristics; (4) the retrieval results are optimized by adjusting the feature weights of similarity measurements according to the user's relevance feedback. The experimental results on NASA data sets can show that our system can achieve comparable superior retrieval performance to existing hyperspectral analysis schemes.

OCIS codes: (100.0100) Image processing; (100.2000) Digital image processing; (110.4234) Multispectral and hyperspectral imaging.

https://doi.org/10.1364/AO.56.004785

1. INTRODUCTION

Imaging spectrometer remote sensing technology was a major breakthrough in the field of earth observation at the end of the last century which can image the same ground objects with several tens to hundreds of spectral bands from ultraviolet to the microwave range [1,2]. The resulting hyperspectral remote sensing image (i.e., hyperspectral image) is far beyond the limits of human vision, and can probe the spatial characteristics of ground objects as well as reflect their subtle spectrum characteristics [3]. It provides a more effective means of analyzing and recognizing ground objects quickly and quantitatively [4,5]. Hyperspectral remote sensing images provide more precise observation information, which also brings a sharp increase in data volume. Therefore, a more efficient technology is necessary for accurately finding the useful information from large-scale hyperspectral remote sensing data. As a result, the content-based image retrieval (CBIR) technology has been conceived [6].

Up to now, most existing CBIR systems focused on panchromatic images or low-dimension multispectral images. In these CBIR systems, images are mostly characterized by low-level visual features, which suppress the accuracy of retrieval results. For example, Ref. [7] realized a CBIR approach for hyperspectral remote sensing images with texture features, which ignores the spectral features. The precision of this method is not explicitly established. Deep learning has been proven to be very effective for many 2D image processing applications [8], especially for large-scale image processing; that is to say, the performance will be significantly improved if the analysis can be applied to image data on a large-scale level. The hyperspectral image can be seen as a 3D data cube, and the size of one file is huge. Nowadays, a general public ground truth database of hyperspectral images has reached a medium size, with more than thousands of images. However, it is far from a large-scale database for deep-learning-based algorithms. Thus, applying deep learning into remote sensing image retrieval is premature so far.

As an emerging field, hyperspectral image retrieval has become a hot research topic. In order to improve retrieval accuracy, researchers focus on extracting precise features. Spectral features are specific to hyperspectral remote sensing images, which plays a decisive role in surface classification. Because of the limitation of spatial resolution, pixels in hyperspectral remote sensing images acquired by hyperspectral imaging

instruments usually contain more than one feature spectrum [9]. Endmembers of hyperspectral images are the image spectral pixels, which are a linear combination of the elementary material signature [10]. They are well suited as a spectral feature, and have been widely applied in many hyperspectral image processing fields, such as image retrieval, image classification, and object detection, etc. The descriptive ability of visual features (such as texture features) of hyperspectral remote sensing images is as good as that of spectral features. This is especially true with texture features, which can serve as a good supplement for the representation of hyperspectral images.

Under the effects of humidity, temperature, light intensity, and other factors, different types of objects may share the same spectral features in some bands, which is called "the same spectrum with different objects" [11]. Some works realize the importance of endmembers, but pay little attention to the above problem. For example, Ref. [12] proposed a spectral-spatial CBIR system for hyperspectral images, in which the endmember induction algorithm (EIA) is utilized to create the endmembers of the image, and the spatial distribution of each endmember is calculated by an unmixing method. Nevertheless, due to the phenomenon in which different objects may share similar spectra, these kinds of hyperspectral images are still difficult to distinguish, even with high spectral resolution. Therefore, classifying the surface only by spectral features is insufficient. In order to represent the image content more accurately, texture feature retrieval is highly desirable.

Similarity measurement is a metric that quantifies the similarity between two images. Most of the existing methods adopt distance measurements such as Euclidean distance [13], Mahalanobis distance [14], and Hamming distance [15], etc. Reference [16] proposed a multiscale space CBIR system for hyperspectral images using integrated spectral and texture features. However, feature similarity is measured with Euclidean distance, which is not appropriate for spectral features. It has been shown that the retrieval results are more inaccurate when the angle between two spectral curves is larger. In other words, traditional distance measurement can directly calculate the distance of two vectors in the feature space, which is more suitable for the texture feature vector of an image. However, the spectral features of hyperspectral images are represented as the spectral curves that do not fit the distance measurement. A spectral matching technique can measure the similarity between spectral curves well, and it is also available to measure the similarity of spectral features. Therefore, it is essential to design a specific similarity measurement method for a hyperspectral remote sensing image retrieval system.

A relevance feedback mechanism can help reduce the semantic gap between image feature representation and user analysis [17]. Reference [18] proposed a relevance feedback mechanism based on the adjustment of feature weights which can assign weights to each feature vector according to the user's evaluation of retrieval results. The experimental results show that this method can improve the retrieval accuracy. Considering the hyperspectral characteristics of spectral imagery and the limited recognizing ability of human vision, it is not feasible to let the user make relevance feedback for returned retrieval results directly. True color synthesis is an effective approach to reproduce the color of actual features as accurately as possible to improve the recognizing ability of human vision.

Based on the aforementioned problems, a hyperspectral remote sensing image retrieval system using spectral and texture features is proposed in this paper. In our work, the feature extractor of hyperspectral remote sensing images is proposed. The spectral features and texture features are extracted by an improved automatic pixel purity index (APPI) algorithm and gray level co-occurrence matrix (GLCM), respectively, to build the feature indexes [19,20]. Then, a similarity measurement method for a hyperspectral remote sensing image retrieval system is designed. The spectral features are measured with the spectral information divergence and spectral angle match (SID-SAM) mixed measurement [21]. Then, the texture features of the image are measured with Image Euclidean Distance (IMED) [22]. Finally, a relevance feedback mechanism is applied to optimize the results, in which principal component analysis (PCA) is utilized to synthesize the true color of spectral imagery, and feature weights are adjusted according to the user's feedback.

The remainder of this paper is organized as follows. In Section 2, the architecture of the proposed hyperspectral remote sensing image retrieval system is provided. Section 3 states the feature extractor of the hyperspectral remote sensing image. The designed similarity measurement method is described in Section 4. Section 5 introduces the proposed retrieval system based on relevance feedback. Experimental results and analysis are given in Section 6. Section 7 provides our conclusions.

2. OVERVIEW OF THE PROPOSED HYPERSPECTRAL REMOTE SENSING IMAGE RETRIEVAL SYSTEM

The architecture of the proposed hyperspectral remote sensing image retrieval system can be divided into two parts: online and offline. The task of the online part is to realize the retrieval process, including the feature extraction, similarity measurement, and relevance feedback. The task of the offline part is to build the feature database of images for similarity matching. The online part includes three steps: (1) building the feature indexes with the extracted spectral features and texture features;

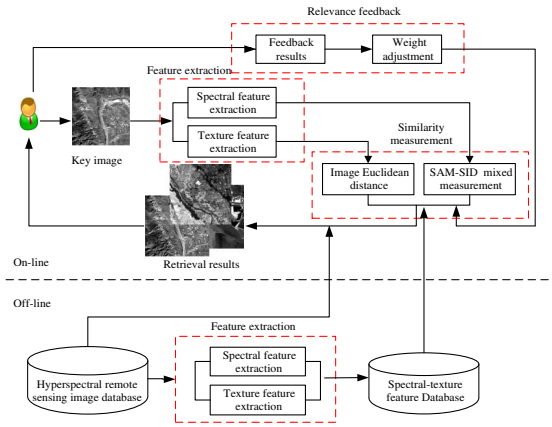

Fig. 1. Flowchart of the proposed hyperspectral remote sensing image retrieval system.

(2) measuring the feature similarities with SID-SAM mixed measurement and IMED, respectively; (3) applying the relevance feedback mechanism to optimize the retrieval results. For the offline part, the features are first extracted from the data in the hyperspectral remote sensing image database, and then used to build the feature database. Figure 1 shows the flowchart of the proposed hyperspectral remote sensing image retrieval system.

3. FEATURE EXTRACTION OF HYPERSPECTRAL REMOTE SENSING IMAGES

In this section, the spectral and texture features of the image are extracted. The endmembers are extracted as the spectral features by an improved APPI algorithm, and the texture features are extracted by GLCM. The hyperspectral remote sensing image can be represented by combining the two features.

A. Endmember Extraction

Endmembers are a spectral signature containing a single material substance which can describe the spectral response of surface features. Therefore, spectral features are spatially invariant; in other words, the spectral signature only related to the material substance. Moreover, spectral features are illumination invariant as well. A spectral signature is a spectral curve which is matched by the shape of the curve. The spectral feature is obtained from the differences between pixels. Here, an endmember is extracted by the improved APPI algorithm, which can be seen in our previous work [19]. First, the number of endmembers is determined with the noise subspace projection (NSP). Then, the image dimension is reduced by improving the method of noise covariance matrix (NCM) estimation for minimum noise fraction (MNF) transformation [23]. We retain 20 components of the transformed images. After projecting these pixels onto the projection vectors, endmembers are extracted from the hyperspectral remote sensing image by finding the pixels located at the extreme positions. The specific procedure is as follows.

Step 1: Dimension number p is determined with the noise subspace projection (NSP).

Step 2: Dimension is reduced by the improved noise covariance matrix (NCM) estimation for MNF transformation, and the counter is set to $n = 1$.

Step 3: To guarantee the comprehensiveness and integrity of the endmember set, K skewers denoted as $\{\text{skewer}_j^{(n)}\}_{j=1}^{K}$ are generated based on the principle of Givens rotation. The rotation angle between two skewers is 15 deg.

Step 4: The pixels located at the extreme positions are found by projecting pixels onto the projection vectors, which will be denoted as the endmembers.

Step 5: Let $\{r_i^{(n)}\}_{i=1}^{N}$ be the i-th sample vector, the total number of sample vectors is N.

Step 6: For each skewer $\text{skewer}_j^{(n)}$, all the data sample vectors are projected onto $\text{skewer}_j^{(n)}$ to find sample vectors at its extreme positions in order to form an extreme set for this particular skewer $\text{skewer}_j^{(n)}$, denoted as $S_{\text{extrema}}(\text{skewer}_j^{(n)})$. Despite the fact that different $\text{skewer}_j^{(n)}$ generate a different extreme set $S_{\text{extrema}}(\text{skewer}_j^{(n)})$, it is highly likely that some sample vectors will appear in more than one extreme set. Define an indicator function $I_s(r_i^{(n)})$ of a set S:

$$I_s(r_i^{(n)}) = \begin{cases} 1; & \text{if } r \in S \\ 0; & \text{if } r \notin S \end{cases} \quad \text{and}$$

$$N_{\text{PPI}}(r_i^{(n)}) = \sum_j I_{S_{\text{extrema}}(\text{skewer}_j^{(n)})}(r_i^{(n)}), \tag{1}$$

where $N_{\text{PPI}}(r_i^{(n)})$ is defined as the pixel purity index (PPI) score of the sample vector $r_i^{(n)}$, which is the times of each pixel located at the extreme positions by projection. Let $\{\text{score}_{\text{PPI}}^{(n)}(j)\}_{j=1}^{p}$ denote the highest PPI scores set, $\text{score}_{\text{PPI}}^{(n)}(j)$ be the j-th highest PPI score.

Step 7: Find a set of sample vectors $E_j^{(n)}$ corresponding to $\text{score}_{\text{PPI}}^{(n)}(j)$. It should be noted that there are generally more than one endmember pixels in the set $E_j^{(n)}$ corresponding to $\text{score}_{\text{PPI}}^{(n)}(j)$; because some pixels are projected to recorded extreme positions more than once. Let $\Omega^{(n)} = \cap_{j=1}^{p} E_j^{(n)}$ be a set of generated endmember pixels at the n-th run.

Step 8: Find $E^{(n)} = \cap_{m=1}^{n} \Omega^{(m)} = \cap_{m=1}^{n} (\cup_{j=1}^{p} E_{j=1}^{(m)})$, the set of endmember pixels up to n, i.e., $1 \le m \le n$.

Step 9: If $E^{(n)} \neq E^{(n-1)}$, it means some endmember pixels have not be recorded yet, then go to **Step 3**; otherwise, the algorithm is terminated. Here, the sample pixel vectors in E^n are represented as the extracted endmembers.

Figure 2 shows the sample images and the results of endmember extraction.

B. Texture Feature Extraction

Texture feature extraction of a hyperspectral image is different from that of a normal image. First, the resolution of a hyperspectral image is much lower than a normal image; second, hyperspectral images contains thousands of times more surface information than a normal image. As a result, the texture features of a hyperspectral image are much more complex.

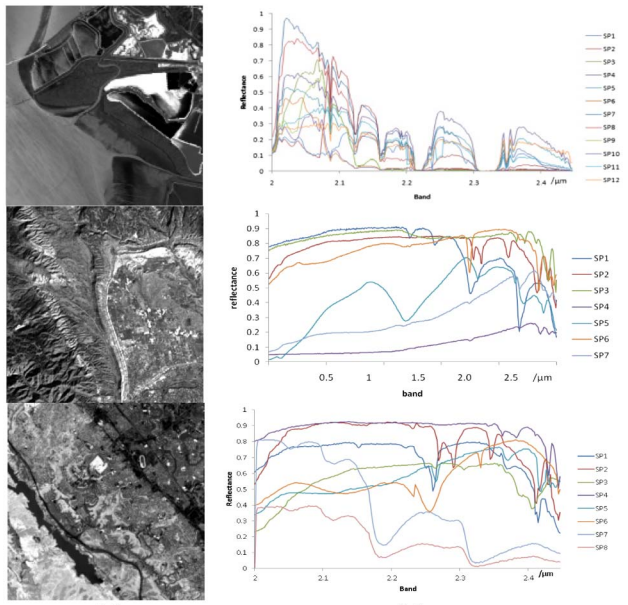

(a) (b)

Fig. 2. Results of endmember extraction: (a) the sample images; (b) the corresponding spectral curves of the extracted endmembers.

The GLCM feature can describe four characteristics: contrast, correlation, energy, and entropy, which are very appropriate for describing the texture features of a hyperspectral image, as well as reflecting the complexity of the texture features. The GLCM is utilized to extract the texture features, and is adapted to analyze the natural geographical characteristics of hyperspectral remote sensing images [24]. It creates a two-dimensional matrix with the same size as the number of gray levels in an image. The GLCM feature matrix is rotation invariant because of its statistical characteristic.

For a 2D texture feature matrix of $N \times N$ pixels with G gray levels, the co-occurrence matrix of $G \times G$ is defined by its gray level and orientation angle θ between the given gray level pairs, which is calculated with a distance vector d. Suppose i and j are the gray values of two pixels in the image $f(x, y)$, and S represents the set of pixel pairs with spatial relation of the image. In this paper, four co-occurrence matrixes are constructed in 0°, 45°, 90°, and 135° with distance $d = 1$:

$$P(i, j, d, 0°) = \text{card}\{[(x_1, y_1), (x_1, y_1 + d)] \in S | f(x_1, y_1) = i \,\&\, f(x_1, y_1 + d) = j\}, \quad (2)$$

$$P(i, j, d, 45°) = \text{card}\{[(x_1, y_1), (x_1 + d, y_1 + d)] \in S | f(x_1, y_1) = i \,\&\, f(x_1 + d, y_1 + d) = j\}, \quad (3)$$

$$P(i, j, d, 90°) = \text{card}\{[(x_1, y_1), (x_1 + d, y_2)] \in S | f(x_1, y_1) = i \,\&\, f(x_1 + d, y_2) = j\}, \quad (4)$$

$$P(i, j, d, 135°) = \text{card}\{[(x_1, y_1), (x_1 - d, y_2)] \in S | f(x_1, y_1) = i \,\&\, f(x_1 - d, y_2) = j\}, \quad (5)$$

where $x_2 = x_1 + d \cos\theta$, $y_2 = y_1 + d \sin\theta$, and card() is the number of the elements with contributions. The four features that can characterize the statistical characteristics of a co-occurrence matrix are extracted, including contrast, correlation, energy, and entropy, as given below [23].

(1) The contrast CON reflects the local variations of texture:

$$\text{CON} = \sum_{i=0}^{L-1} \sum_{j=0}^{L-1} (i - j)^2 P(i, j), \quad (6)$$

where i and j are the gray values, L is the gray level, and $P(i, j)$ is the joint probability density.

(2) The correlation COR represents the linear dependency between gray levels in the texture, which is defined as

$$\text{COR} = \frac{\sum_{i=0}^{L-1} \sum_{j=0}^{L-1} ijP(i, j) - \mu_x \mu_y}{\sigma_x \sigma_y}, \quad (7)$$

where μ_x, μ_y and σ_x, σ_y are the means and standard deviations of the marginal distributions associated with the co-occurrence matrix, respectively.

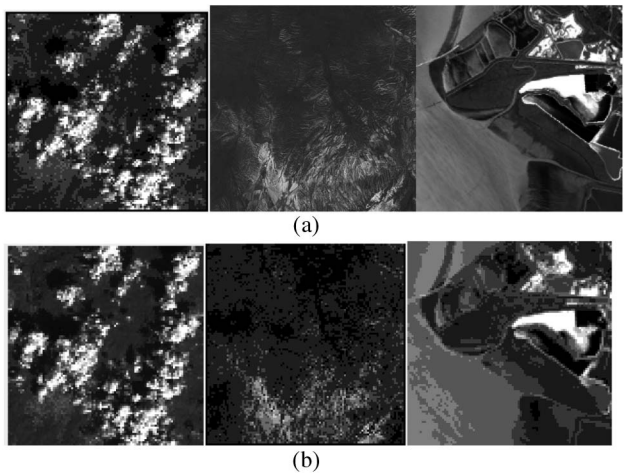

Fig. 3. Results after GLCM: (a) original data; (b) feature images.

(3) The energy ASM measures the textural homogeneity:

$$\text{ASM} = \sum_{i=0}^{L-1} \sum_{j=0}^{L-1} P^2(i, j). \quad (8)$$

(4) The entropy ENT indicates the disorder of the texture:

$$\text{ENT} = -\sum_{i=0}^{L-1} \sum_{j=0}^{L-1} P(i, j) \log P(i, j). \quad (9)$$

Finally, the texture feature of the hyperspectral remote sensing image is extracted by GLCM. Figure 3 shows the results of the texture feature extraction. The original data are shown in Fig. 3(a) and the obtained feature images are shown in Fig. 3(b).

4. SIMILARITY MEASUREMENT FOR THE HYPERSPECTRAL REMOTE SENSING IMAGE

Because hyperspectral remote sensing images contain both spectral and texture features, a similarity measurement for the hyperspectral remote sensing image retrieval system is designed in this section. First, the spectral features are measured though the SID-SAM mixed measurement. Then, the texture features are measured by IMED for the second match. Figure 4 shows the flowchart of the similarity measurement for our hyperspectral remote sensing image retrieval system.

A. SID-SAM Mixed Measurement

Hyperspectral remote sensing images contain hundreds of narrow and contiguous spectral bands, with wavelengths ranging from the visible spectrum to the infrared spectrum. In this

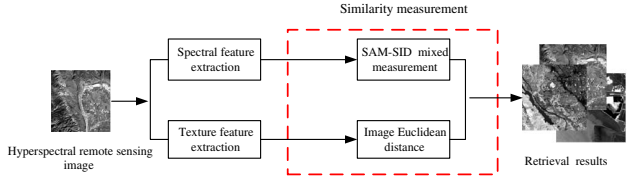

Fig. 4. Flowchart of the similarity measurement for our hyperspectral remote sensing image retrieval system.

paper, SID-SAM mixed measurement is utilized to measure the similarity of spectral features [20] between key images and images in a database. The procedures can be summarized as follows.

Step 1: Suppose two hyperspectral remote sensing images pixel vectors are $\mathbf{r} = (r_1, r_2, \ldots, r_L)^{\mathrm{T}}$ and $\mathbf{r}' = (r'_1, r'_2, \ldots, r'_n)^{\mathrm{T}}$, in which the components r_i and r'_i represent the pixels in the band images B_i and B'_i.

Step 2: The respective spectral signatures of the two images are denoted as $\mathbf{s} = (s_1, s_2, \ldots, s_L)^{\mathrm{T}}$ and $\mathbf{s}' = (s'_1, s'_2, \ldots, s'_L)^{\mathrm{T}}$, in which $\mathbf{s}$ represents the spectral signature of $\mathbf{r}$ in the form of either radiance or reflectance values.

Step 3: Let $\mathbf{p} = (p_1, p_2, \ldots, p_L)^{\mathrm{T}}$ and $\mathbf{q} = (q_1, q_2, \ldots, q_L)^{\mathrm{T}}$ be the two probability mass functions generated by $\mathbf{s}$ and $\mathbf{s}'$, respectively. The self-information I for pixel vector $\mathbf{r}$ and vector $\mathbf{r}'$ of band I are defined as

$$I_i(\mathbf{r}) = -\log p_i, \tag{10}$$

$$I_i(\mathbf{r}') = -\log q_i. \tag{11}$$

Step 4: Calculate the discrepancy $D(\mathbf{r}\|\mathbf{r}')$ in the self-information of the band image B_i in $\mathbf{r}$ relative to the self-information of B_i in $\mathbf{r}'$, which can be denoted as

$$D(\mathbf{r}\|\mathbf{r}') = I_i(\mathbf{r}) - I_i(\mathbf{r}') = \log(p_i/q_i). \tag{12}$$

Step 5: Average $D_i(\mathbf{r}\|\mathbf{r}')$ over all the band images $\{B_L\}_{l=1}^{L}$ with respect to $\mathbf{r}$ results in

$$D(\mathbf{r}\|\mathbf{r}') = \sum_{i=1}^{L} D(\mathbf{r}\|\mathbf{r}')p_i = \sum_{i=1}^{L} p_i \log(p_i/q_i), \tag{13}$$

where $D(\mathbf{r}\|\mathbf{r}')$ is the average discrepancy in the self-information of $\mathbf{r}'$ relative to that of $\mathbf{r}$. Similarly, the average discrepancy in the self-information of $\mathbf{r}$ relative to the self-information of $\mathbf{r}'$ can be defined by

$$D(\mathbf{r}'\|\mathbf{r}) = \sum_{i=1}^{L} D(\mathbf{r}'\|\mathbf{r})q_i = \sum_{i=1}^{L} q_i \log(q_i/p_i). \tag{14}$$

Step 6: Calculate the spectral information divergence (SID), which can be obtained by adding Eqs. (13) and (14) as follows:

$$\mathrm{SID}(\mathbf{r}, \mathbf{r}') = D(\mathbf{r}\|\mathbf{r}') + D(\mathbf{r}'\|\mathbf{r}), \tag{15}$$

where the $\mathrm{SID}(\mathbf{r}, \mathbf{r}')$ can be used to measure the discrepancy between two pixel vectors $\mathbf{r}$ and $\mathbf{r}'$ in terms of their corresponding probability mass functions $\mathbf{p}$ and $\mathbf{q}$.

Step 7: The spectral angle mapper (SAM) measures the spectral similarity by finding the angle between the spectral signatures $\mathbf{s}$ and $\mathbf{s}'$ of two pixel vectors $\mathbf{r}$ and $\mathbf{r}'$,

$$\mathrm{SAM}(\mathbf{s}, \mathbf{s}') = \cos^{-1}\left(\frac{\langle \mathbf{s}, \mathbf{s}' \rangle}{\|\mathbf{s}\|\|\mathbf{s}'\|}\right), \tag{16}$$

where $\langle \mathbf{s}, \mathbf{s}' \rangle = \sum_{l=1}^{L} s_l s'_l$, $\|\mathbf{s}\| = (\sum_{l=1}^{L} s_L^2)^{1/2}$. The s_l can represent the spectral signature of r_l in the form of either radiance or reflectance values.

Step 8: The SID-SAM mixed measurement S is obtained by multiplying the SID with the tangent of the SAM between two spectral signatures $\mathbf{s}$ and $\mathbf{s}'$, which is given by

$$S = \mathrm{SID}(\mathbf{r}, \mathbf{r}') \times \tan(\mathrm{SAM}(\mathbf{r}, \mathbf{r}')). \tag{17}$$

B. IMED

IMED is used to measure the similarity of texture features, which is based on the kernel function [21]. The specific procedures are as follows.

Step 1: Assume that $e_1, e_2, \ldots, e_{M\times N}$ is a set of basis of images, the measure coefficient g_{ij} is given by

$$g_{ij} = \langle e_i, e_j \rangle = \sqrt{\langle e_i, e_i \rangle} \cdot \sqrt{\langle e_j, e_j \rangle} \cdot \cos\theta_{ij}. \tag{18}$$

If the lengths of the basis are equal, the distance d between image x and y can be denoted as

$$d(x, y) = \left(\sum_{i,j=1}^{M\times N} g_{ij}(x^i - y^i)(x^j - y^j)\right)^{1/2} = ((x-y)^T \mathbf{G}(x-y))^{1/2}, \tag{19}$$

where $\mathbf{G} = (g_{ij})_{MN\times MN}$ is the measure matrix, which is required to satisfy the following three conditions.

a) The measure coefficient g_{ij} decided by the distance between P_i and P_j is defined as

$$g_{ij} = f(|P_i - P_j|) \qquad i, j = 1, 2, \ldots, M \times N. \tag{20}$$

b) The function f is a continuous function that decreases with the increase of the distance between P_i and P_j.

c) The function f is suitable for images with any size and resolution.

Based on the above conditions, the Gauss function is chosen to be the function f in this paper. The measure coefficient g_{ij} can be expressed as

$$g_{ij} = f(|P_i - P_j|) = \frac{1}{2\pi\sigma^2} \exp\left(\frac{-|P_i - P_j|^2}{2\sigma^2}\right). \tag{21}$$

Step 2: Let $\sigma = 1$; the IMED d_{IMED} is then given as

$$d_{\mathrm{IMED}}(x, y) = \left(\frac{1}{2\pi}\sum_{i,j=1}^{M\times N} \exp\left(\frac{-|P_i - P_j|^2}{2}\right)(x^i - y^i)(x^j - y^j)\right)^{1/2}. \tag{22}$$

Step 3: Make the eigenvalue decomposition for $\mathbf{G} = (g_{ij})_{MN\times MN}$

$$\mathbf{G} = \mathbf{\Gamma}^T \Lambda \mathbf{\Gamma}, \tag{23}$$

where Λ is the diagonal matrix composed by the eigenvalues of $\mathbf{G}$, and $\mathbf{\Gamma}$ is the orthogonal matrix composed by the feature vector. Make standard transformation for $\mathbf{G}$ as follows:

$$\mu = \mathbf{G}^{1/2} x, \tag{24}$$

$$v = \mathbf{G}^{1/2} y, \tag{25}$$

where $\mathbf{G}^{1/2} = \mathbf{\Gamma}^T \Lambda^{1/2} \mathbf{\Gamma}$.

The IMED d_{IMED} can be denoted as

$$d_{\mathrm{IMED}}((x-y)^T \mathbf{G}(x-y))^{1/2} = ((\mu - v)^T(\mu - v))^{1/2}. \tag{26}$$

5. HYPERSPECTRAL REMOTE SENSING IMAGE RETRIEVAL SYSTEM BASED ON USER FEEDBACK

As mentioned, true color synthesis can be used to improve the recognizing ability of human vision. In this paper, the true color

of hyperspectral remote sensing images is synthesized with a PCA-based method. Then, the relevance feedback is performed by adjusting feature weights.

A. True Color Synthesis Method Based on PCA Transformation

Based on the principle of color synthesis, true color synthesis for hyperspectral remote sensing images provides an effective means of synthesizing the RGB image of multispectral data. The red, green, and blue in a synthesized image correspond to three bands of hyperspectral data. After synthesis, image features can be displayed with different colors, which is more in accord with human observing habits and easy to distinguish.

The PCA transformation is a linear transformation which can project the original high-dimensional data to a new coordinate space [25]. The components with little information will be discarded after they are transformed. However, the principal components that contain more information will be retained. The remaining transformed principal components are unrelated to each other. Reference [26] proposed a true color synthesis method based on PCA transformation which takes the advantages of flexible spectral band selection with less loss of spectral information.

Based on Ref. [26], true color synthesis is first performed on the hyperspectral remote sensing images before users execute the evaluation and the feedback on the synthetic images directly. Figure 5 shows the flowchart of the true color synthesis method based on PCA transformation. The true color synthesis based on PCA transformation can be reviewed as follows.

Step 1: Transform the image with PCA. For a sample set $\mathbf{X}$, the number of samples is n, and each sample contains P variables. The sample set $\mathbf{X}$ can be expressed as

$$\mathbf{X} = \begin{bmatrix} x_{11} & x_{12} & \cdots & x_{1p} \\ x_{21} & x_{22} & \cdots & x_{2p} \\ \vdots & \vdots & \ddots & \vdots \\ x_{p1} & x_{p2} & \cdots & x_{pp} \end{bmatrix} = [X_1, X_2, \ldots, X_p]. \quad (27)$$

By performing the PCA transformation for the hyperspectral image with p bands, the independent principal components can be obtained. The correlation matrix $\mathbf{R} = (r_{ij})_{p\times p}$ is defined as

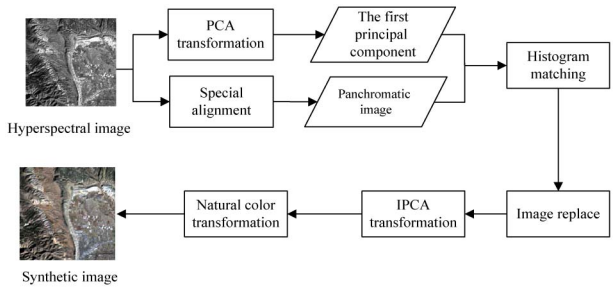

Fig. 5. Flowchart of true color synthesis method based on PCA transformation.

$$\mathbf{R} = \begin{bmatrix} r_{11} & r_{12} & \cdots & r_{1p} \\ r_{21} & r_{22} & \cdots & r_{2p} \\ \vdots & \vdots & \ddots & \vdots \\ r_{p1} & r_{p2} & \cdots & r_{pp} \end{bmatrix}, \quad (28)$$

$$r_{ij} = \frac{\sum_{k=1}^{n}(x_{ki} - \bar{x}_i)(x_{kj} - \bar{x}_j)}{\sqrt{\sum_{k=1}^{n}(x_{ki} - \bar{x}_i)^2 \sum_{k=1}^{n}(x_{kj} - \bar{x}_j)^2}}, \quad (29)$$

where x_{ki} is the pixel of the sample. According to the characteristic equation $|\lambda\mathbf{I} - \mathbf{R}|$, the eigenvalues $\{\lambda_1 \geq \lambda_2 \geq \cdots \geq \lambda_p\}$ and eigenvector $\varphi_i (i = 1, 2, \ldots, p)$ can be obtained. Let $\sum_{j=1}^{p} \varphi_{ij}^2 = 1$, and φ_{ij} is the j-th component of φ_i. The transformation matrix $\mathbf{W}$ of PCA can be denoted as

$$\mathbf{W} = [\varphi_1, \varphi_2, \ldots, \varphi_p]. \quad (30)$$

The principal component $\mathbf{C}_k$ of the image can be obtained by

$$\mathbf{C}_k = \sum_{i=p}^{n} d_i \varphi_{ik}, \quad (31)$$

where $k (k = 1, 2, \ldots, n)$ is the ordinal of the principal component, $\mathbf{C}_k$ is the k-th principal component, i is the input band, P is the total number of bands, d_i is the data value of the i-th band of the image, and φ_{ik} is the element of the i-th row and k-th column in the eigenvector matrix.

Step 2: Perform the spatial alignment to calculate the mapping relationship between the spatial coordinates and the gray level of the two images. Suppose I_A and I_B are the reference image and input image, respectively, and $I_A(x, y)$ and $I_B(x, y)$ are the pixel gray-value in pixel (x, y) of two images, which can be expressed as

$$I_A(x, y) = g(I_B(f(x, y))), \quad (32)$$

where g represents the gray scale transformation. The coordinate transformation f is decided by the coordinate transformation of reference image and input image, which is given by

$$f(x, y) = (x', y'). \quad (33)$$

The coordinate transformation of two images can be obtained with a rigid transformation,

$$\begin{pmatrix} x' \\ y' \end{pmatrix} = \begin{pmatrix} \cos\theta & -\sin\theta \\ \sin\theta & \cos\theta \end{pmatrix} \begin{pmatrix} x \\ y \end{pmatrix} + \begin{pmatrix} t_x \\ t_y \end{pmatrix}, \quad (34)$$

where θ is the rotation angle, and t_x and t_y are the shift values. In this way, the panchromatic image is obtained.

Step 3: Perform the histogram matching between the panchromatic image and the first principal component to ensure the gray mean and variance are consistent. The histogram matching technique is the transformation of an image so that its histogram matches a specified histogram [27]. We calculate the cumulative distribution functions of the two images' histograms, which can be expressed as $F_1(\cdot)$ and $F_2(\cdot)$. Then, for each gray level $G_1 \in [0, 255]$, we find the gray level G_2 that satisfies the $F_1(G_1) = F_2(G_2)$. The histogram matching function is defined as

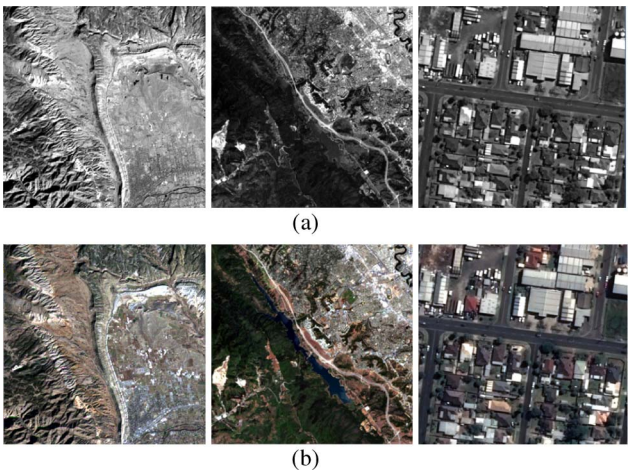

Fig. 6. Results after true color synthesis: (a) original data; (b) data after true color synthesis.

$$M(G_1) = G_2. \tag{35}$$

Step 4: Replace the first principal component with the image generated by histogram matching. Then perform the inverse principal components analysis (IPCA) transformation. The transformed image $\mathbf{Y}$ can be obtained by

$$\mathbf{Y} = \mathbf{W}^{\mathrm{T}} \cdot \mathbf{C}_k, \tag{36}$$

where $\mathbf{C}_k$ is the k-th principal component of image, and $\mathbf{W}^{\mathrm{T}}$ is the transposition of the characteristic matrix $\mathbf{W}$.

Step 5: Perform the natural color transformation, Band_1, Band_2, and Band_3, as three input bands of image fusion, in which these represent the near-infrared band, red band, and green band, respectively. Band_4 represents the output band, which can be expressed as

$$\mathrm{Band}_4 = (\mathrm{Band}_1 \times \mathrm{Band}_3)/4. \tag{37}$$

Finally, the synthetic image is obtained by combining the Band_2, Band_4, and Band_1 in the RGB color space.

Figure 6 shows the results of the true color synthesis method based on PCA transformation. As can be seen, the observation for ground objects is more precise in the synthetic images. For example, the textures of the river and vegetation are clearer in Fig. 6(b) than Fig. 6(a).

B. Relevance Feedback Mechanism Based on Adjustment of Feature Weights

After true color synthesis, the relevance feedback mechanism is implemented to improve the performance of the system. The relevance feedback mechanism based on the adjustment of feature weights can assign weights to each feature vector according to the user's evaluation on the retrieval results [18]. The feature vector that is more similar to the key image is labeled with a higher weight. Then the similarity between images should be recalculated once the weights are adjusted.

In this paper, we will adjust the statistical measure weights of spectral features and the texture feature. The principle of the feature weights adjustment method is shown in Fig. 7, which can be described as follows.

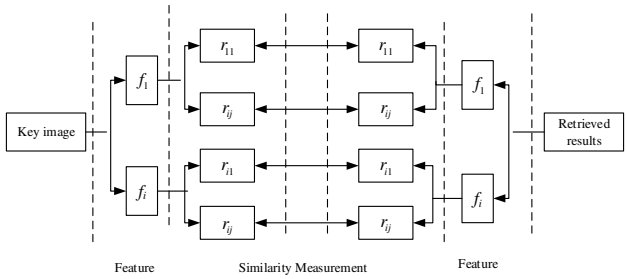

Fig. 7. Principle of the feature weights adjusting method.

Step 1: Assume the image retrieval model as $\mathbf{O}(\mathbf{D}, \mathbf{F}, \mathbf{R}, \mathbf{M})$, $\mathbf{D}$ is the original data, $\mathbf{F} = \{f_i\}$ represents the visual feature set of image, $\mathbf{R} = \{r_{ij}\}$ represents some specific feature, and $\mathbf{M}$ is the similarity model. Initialize the weight vector $\mathbf{W} = [\mathbf{W}_i, \mathbf{W}_{ij}, \mathbf{W}_{ijk}]$,

$$\begin{cases} \mathbf{W}_i = \mathbf{W}_{oi} = \frac{1}{I} \\ \mathbf{W}_{ij} = \mathbf{W}_{oij} = \frac{1}{J_i} \\ \mathbf{W}_{ijk} = \mathbf{W}_{oijk} = \frac{1}{K_{ij}} \end{cases}, \tag{38}$$

where I is the number of visual feature sets $\mathbf{F}$, J_i is the dimension of feature vector f_i, and K_{ij} is the length of r_{ij}.

Step 2: The features of image Q selected by users are extracted and expressed as a linear combination of feature vector f_i with different weights. Each f_i is a linear combination of r_{ij} with different weights.

Step 3: The similarity between key image and retrieval result is denoted as $S(r_{ij})$:

$$S(r_{ij}) = m_{ij}(r_{ij}, \mathbf{W}_{ijk}). \tag{39}$$

Step 4: The similarity of some certain features is $S(f_i)$, which can be expressed as

$$S(f_i) = \sum_j \mathbf{W}_{ij} S(r_{ij}). \tag{40}$$

Step 5: Hence, the total similarity S can be expressed as

$$S = \sum_i \mathbf{W}_i S(f_i). \tag{41}$$

Step 6: The images are ranked according to the similarity with the key image. Then the Top-N images are returned to the user as the retrieval results.

Step 7: Users can evaluate the returned results for five levels, let T be the set of Top-N images, and the evaluation scores S_{TL} of image T_L are given by

$$S_{\mathrm{TL}} \begin{cases} 3, & \text{Highly Relevant} \\ 1, & \text{Relevant} \\ 0, & \text{No-Opinion} \\ -1, & \text{Non-Relevant} \\ -3, & \text{Highly Non-Relevant} \end{cases}. \tag{42}$$

Step 8: Suppose $T_{ij,l}$ is the most similar image to the key image, then the weight vector $\mathbf{W}_{ij}$ can be adjusted as the following:

$$\mathbf{W}_{ij} = \begin{cases} \mathbf{W}_{ij} + S_{Tl} & \text{if } T_{ij,l} \in T_l \\ \mathbf{W}_{ij} & \text{else} \end{cases}. \quad (43)$$

Step 9: Estimate the weight vector $\mathbf{W}_{ijk}$ as the following:

$$\mathbf{W}_{ijk} = \frac{1}{\sigma_{ijk}}, \quad (44)$$

where the standard deviation of the sequence is denoted by r_{ij}. Then go to **Step 2** and start the new round of retrieval.

6. EXPERIMENTAL RESULTS AND ANALYSIS

In this section, a quantitative study and comparative analysis are conducted to demonstrate the effectiveness of the proposed hyperspectral remote sensing image retrieval system based on spectral and texture features. In the first experiment, the texture features of different objects with similar spectra are analyzed to address the problem of "the same spectrum with different objects." In the second experiment, the weighting method in Ref. [28], the average method in Ref. [29], and the PCA-based method in Ref. [30] are compared to verify the performance of the true color synthesis method used in this paper. In the third experiment, the results before and after applying the relevance feedback mechanism on the proposed retrieval system are compared. In the fourth experiment, the retrieval results of spectral-spatial method in Ref. [12], the endmember-based method in Ref. [31], the multiscale space method in Ref. [16], and the proposed retrieval system are compared.

A. Experimental Data Set and Setting

We conducted experiments on a collection of the high-resolution hyperspectral remote sensing data sets obtained from the German Aerospace Center (DLR) in Oberfaffenhofen, Germany and the NASA over the World Trade Center (WTC) area in New York. The airborne visible infrared imaging spectrometer (AVIRIS) images contain 125 spectral bands between 0.4 and 2.5 mm. The spatial resolution is 20 m, and the spectral resolution is 10 nm. The experimental platform is a PC with 2.10 GHz CPU, 5.00G memory, Windows 7 operating system. Figure 8 shows several sample images with 64×64 pixels. Our data set contains 3000 hyperspectral remote sensing images, which roughly fall into five categories: city, forest, water, meadow, and rocks.

B. Experiment I

To address the problem of "the same spectrum with different objects," the texture features of different objects with similar spectra are analyzed. Figure 9 shows two hyperspectral remote sensing images, both containing a water area: a river in Fig. 9(a) and a lake in Fig. 9(b). Although the two images have the materials of "water" with the same spectrum, the texture feature is different.

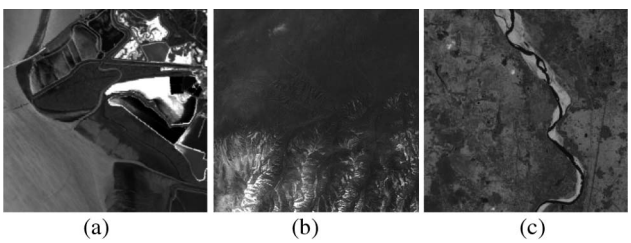

Fig. 8. Sample AVIRIS images.

Fig. 9. Two hyperspectral remote sensing images: (a) river image; (b) lake image.

The improved APPI algorithm is utilized to extract the spectral features of the two images, and the spectral curves of the river and lake are shown in Fig. 10.

As can be seen from Fig. 10, the spectral curves of the two objects with same material are very similar, so it is difficult to distinguish them only by spectral features. Next, the texture features of the images are extracted by GLCM, and the resulting statistic of the texture features of the two examples are given in Table 1.

It can be seen from Table 1 that the statistics of the texture features of the two images vary widely. Hence, the texture features of the image can help distinguish objects when the spectral features are similar. That is to say, the proposed feature extraction of hyperspectral remote sensing images can help solve the problem of "the same spectrum with different objects."

C. Experiment II

For hyperspectral image retrieval, the spectral information is difficult to be distinguishable by the human visual system. Therefore, if we only use the original hyperspectral images in relevance feedback, the resultant performance may not be satisfactory. In this experiment, three true color synthesis methods are compared to verify the performance of the proposed method. The weighting method [28], the average method [29], and the PCA-based method [30] are conducted on the hyperspectral remote sensing image for true color synthesis.

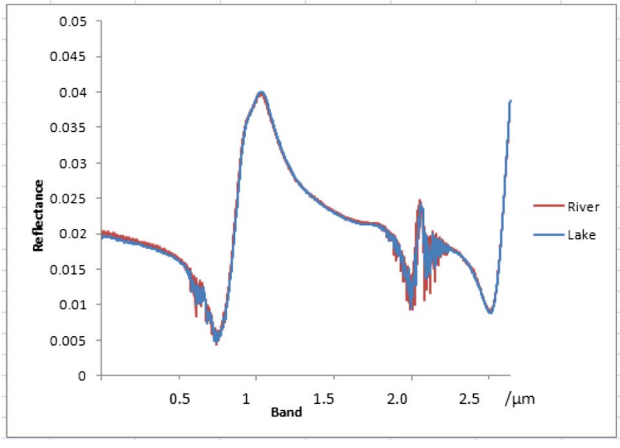

Fig. 10. Spectral curves of the two materials.

Table 1. Statistics of the Texture Features

Statistic	Contrast	Correlation	Energy	Entropy
River image	67.32	-1.5×10^{21}	3.65×10^{-3}	6.54
Lake image	48.19	-3.2×10^{21}	1.83×10^{-2}	9.81

Figure 11 shows the results of true color synthesis. It can be seen that the color deviation of the actual object is huge in Fig. 11(a), and the color of residential areas is distorted in Fig. 11(b). Moreover, the synthesis result of Fig. 11(c) is closest to the actual object, and that property can further improve the ability of human eye identification.

For further demonstration, the amount of information in the synthesis image is used to analyze our synthesis results quantitatively.

1. Mean and Standard Deviation

Based on statistical theory, the mean μ and the standard deviation σ can be defined as

$$\mu = \frac{1}{n}\sum_{i=1}^{n} x_i, \tag{45}$$

$$\sigma = \sqrt{\frac{1}{n-1}\sum_{i=1}^{n}(x_i - \mu)^2}, \tag{46}$$

where n is the total number of samples, and x_i is the i-th sample.

2. Entropy and Joint Entropy

According to the Shannon theorem, for the image x with L gray levels $\{0, 1, \ldots, L-1\}$, the entropy $H(x)$ can be expressed as

$$H(x) = -\sum_{i=0}^{L-1} P_i \log_2 P_i, \tag{47}$$

where P_i represents the probability of a gray level i in the image. The joint entropy of two images $H(x_1, x_2)$ and the joint entropy of three images $H(x_1, x_2, x_3)$ can be expressed as

$$H(x_1, x_2) = -\sum_{i_1, i_2=0}^{L-1} P_{i_1,i_2} \log_2 P_{i_1,i_2}, \tag{48}$$

$$H(x_1, x_2, x_3) = -\sum_{i_1, i_2, i_3=0}^{L-1} P_{i_1,i_2,i_3} \log_2 P_{i_1,i_2,i_3}, \tag{49}$$

where i_1 is the pixel gray value of image x_1, i_2 is the pixel gray value of image x_2, P_{i_1,i_2} is the joint probability of x_1 and x_2. P_{i_1,i_2,i_3} is the joint probability of x_1, x_2, and x_3.

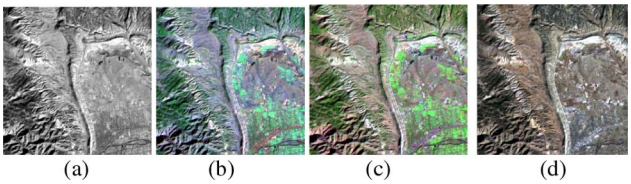

(a) (b) (c) (d)

Fig. 11. Results of true color synthesis: (a) original data; (b) average method; (c) weighting method; (d) PCA-based method.

The image contains more information if the entropy is larger. Table 2 gives the amount of information of the synthesis image for the three different methods.

As can be seen from Table 2, compared with the average method and the weighting method, the joint entropy and the mean value of the image obtained by the PCA-based method perform best. For the joint entropy of Band_1, the joint entropy values obtained by the average method and the weighting method are 14.792 and 15.658, respectively. However, the entropy is 16.397 by the PCA-based method. Therefore, the PCA-based method can retain the inherent high spatial resolution while demonstrating less spectral distortion.

D. Experiment III

In this experiment, we compare the retrieval performance before and after relevance feedback. Ten users participated in the relevance feedback, including staff and students with at least two years' experience of image processing. Each participant performed more than 1000 queries on the image data set, which contains more than 3000 hyperspectral remote sensing images. To avoid potential collaboration, each participant made the evaluation independently. The interface of the proposed hyperspectral remote sensing image retrieval system and the corresponding retrieval results are shown in Figs. 12 and 13.

As can be seen, the visual quality of the image is improved obviously after true color synthesis, which is more suitable for observation. The retrieval performance usually adopts precision and recall as the evaluation criteria [6]. In this paper, we defined

Table 2. Amount of Information of the Synthesis Image by Three Different Methods

Method	Band	Entropy	Joint Entropy	Mean	Standard Deviation
Average method	1	6.041	14.792	173.483	68.342
	2	5.163		172.847	67.434
	3	5.272		172.429	67.121
Weighting method	1	6.482	15.658	173.583	68.521
	2	5.937		172.845	67.435
	3	5.385		173.241	68.143
PCA-based method	1	7.093	16.397	172.928	68.046
	2	6.745		173.536	68.654
	3	6.891		173.445	68.462

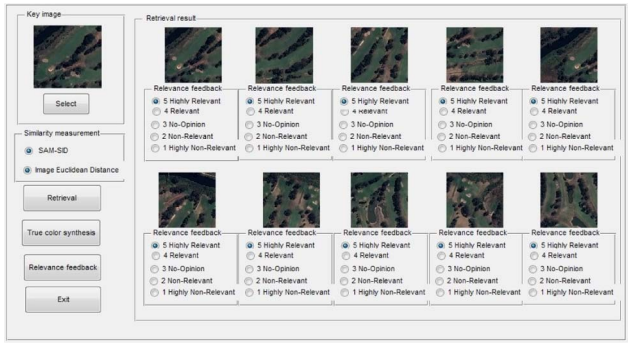

Fig. 12. Interface of the proposed hyperspectral remote sensing image retrieval system.

Fig. 13. Retrieval results of the proposed hyperspectral remote sensing image retrieval system using spectral and texture feature: (a) key image; (b) retrieval results.

the number of retrieved similar images as SIR, the number of retrieved non-similar images as NSIR, and the number of non-retrieved similar images as SINR. The definition of precision and recall can be denoted as

$$\text{Precision} = \frac{\text{SIR}}{\text{SIR} + \text{NSIR}}, \tag{50}$$

$$\text{Recall} = \frac{\text{SIR}}{\text{SIR} + \text{SINR}}. \tag{51}$$

Precision reflects the accuracy of a retrieval algorithm, while recall reflects the comprehensiveness of the algorithm. Figure 14 illustrates the recall-precision curves of the proposed system before and after relevance feedback, in which the vertical axis is the precision ratio and the horizontal axis is the recall ratio.

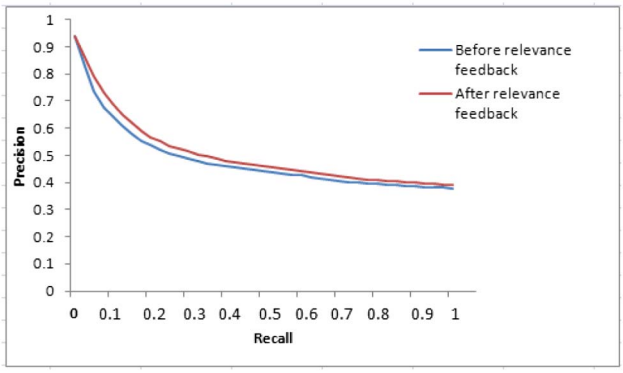

Fig. 14. Precision-recall curves before and after relevance feedback.

As can be seen from Fig. 14, the recall-precision ratio curve of the proposed system after relevance feedback is higher. The corresponding precision ratios can be obtained by Eq. (50), and the data are given in Table 3.

As can be seen from Table 3, the precision ratio of the proposed system before relevance feedback is 80.32%, while it achieved 82.53% after relevance feedback. Hence, the performance of the proposed system can be improved by introducing a relevance feedback mechanism.

E. Experiment IV

To demonstrate the effectiveness of the proposed system, the spectral-spatial method in Ref. [12], the endmember-based method in Ref. [31], and the multiscale space method in Ref. [16] are compared. The precision-recall curves are shown in Fig. 15, in which the vertical axis is the precision ratio and the horizontal axis is the recall ratio.

As can be seen from Fig. 15, four curves with different colors are shown, i.e., the precision-recall ratio of the spectral-spatial

Table 3. Average Precision Ratios Before and After Relevance Feedback

Method	Before Relevance Feedback	After Relevance Feedback
Precision ratio	80.32%	82.53%

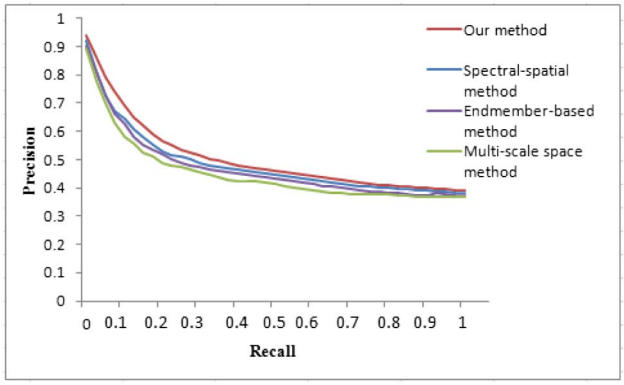

Fig. 15. Precision-recall curves of four different methods.

Table 4. Average Precision Ratios of Four Different Methods

Method	Endmember-Based Method in Ref. [31]	Spectral-spatial Method in Ref. [12]	Multiscale Space Method in Ref. [16]	Our Method
Precision ratio	73.04%	73.22%	74.16%	82.53%

Table 5. Time Cost of the Hyperspectral Image Retrieval System

Online	Offline
4.1 s	12,300 s

method in Ref. [12], endmember-based method in Ref. [31], the multiscale space method in Ref. [16], and our method. The curve of our method is the highest. These corresponding precision ratios are given in Table 4.

As can be seen from Table 4, the performance of our method is 82.53%, which is superior to 73.04% in Ref. [31], 73.22% in Ref. [12], and 74.16% in Ref. [16]. The precision ratio has increased by 12.9%, 12.7%, and 11.3%, respectively. This further shows that our method makes full use of the features of hyperspectral remote sensing images and has the better performance.

As can be seen from Table 5, the online time cost for retrieving a hyperspectral image is 4.1 s, which is more time than a normal image retrieval. This is because the hyperspectral image contains images of hundreds of bands. Therefore, the time cost is also hundreds of times more than the normal image retrieval. In future work, we will further improve the computational efficiency of our method.

7. CONCLUSIONS

In this paper, a hyperspectral remote sensing image retrieval system using spectral and texture features has been proposed. First, a feature extraction method of hyperspectral remote sensing images is proposed. The improved APPI algorithm is utilized to extract endmembers, i.e., spectral features. Then, the texture features are extracted with the GLCM. Next, the similarity measurement for the hyperspectral remote sensing image retrieval system is designed. The spectral features and textural features are measured though SID-SAM mixed measurement and IMED, respectively. Finally, a relevance feedback mechanism based on feature weights adjustment is introduced. PCA is utilized to synthesize true color of spectral imagery, and the feature weights are adjusted according to the user's feedback data to optimize the retrieval results. The experimental results show that the proposed system can achieve comparable or superior retrieval performance. However, the computational complexity is the disadvantage of this method. In future work, more features of hyperspectral remote sensing images will be applied to the hyperspectral image data sets. Deep learning has become so popular in recent years, having seen the rich achievements that deep learning has gained in 2D images, and considering the special structure of hyperspectral images. We will thoroughly consider all kinds of situations which may occur when applying deep learning into hyperspectral image retrieval. Furthermore, we will carry out hyperspectral image analysis in deep learning after coming up with relatively mature technical ideas.

Funding. National Natural Science Foundation of China (NSFC) (61370189, 61531006, 61372149, 61471013); Natural Science Foundation of Beijing Municipality (4163071); Importation and Development of High-Caliber Talents Project of Beijing Municipal Institutions (CIT&TCD20150311); Funding Project for Academic Human Resources Development in Institutions of Higher Learning Under the Jurisdiction of Beijing Municipality.

REFERENCES

1. A. Plaza, J. A. Benediktsson, J. W. Boardman, J. Brazile, L. Bruzzone, G. Camps-Valls, J. Chanussot, M. Fauvel, P. Gamba, A. Gualtieri, M. Marconcini, J. C. Tilton, and G. Trianni, "Recent advances in techniques for hyperspectral image processing," Rem. Sensing Environ. **113**, S110–S122 (2009).
2. R. O. Green, M. L. Eastwood, C. M. Sarture, T. G. Chrien, M. Aronsson, B. J. Chippendale, J. A. Faust, B. E. Pavri, C. J. Chovit, M. Solis, M. R. Olah, and O. Williams, "Imaging spectroscopy and the airborne visible/infrared imaging spectrometer (AVIRIS)," Rem. Sensing Environ. **65**, 227–248 (1998).
3. L. Wang, F. Wei, and D. Liu, "Endmember extraction based on modified iterative error analysis," in *IEEE International Geoscience and Remote Sensing Symposium* (IEEE, 2013), pp. 1071–1074.
4. J. Zhang, W. Geng, L. Zhuo, Q. Tian, and Y. Cao, "Multiscale target extraction using a spectral saliency map for a hyperspectral image," Appl. Opt. **55**, 8089–8100 (2016).
5. O. Abílio, C. Júnior, P. R. Meneses, and R. F. Guimarães, "Analysis absorption band positioning: a new method for hyperspectral image treatment," in *Proceedings of (2001) AVIRIS Workshops*, Pasadena, California, USA, 27 February–2 March 2001, pp. 59–65.
6. A. J. Plaza, "Content-based hyperspectral image retrieval using spectral unmixing," Proc. SPIE **XVII**, 547–556 (2011).
7. B. Demir and L. Bruzzone, "A novel active learning method in relevance feedback for content-based remote sensing image retrieval," IEEE T. Geosci. Remote Sens. **53**, 2323–2334 (2015).
8. X. G. Wang, D. Xiong, and B. Xiang, "Deep sketch feature for cross-domain image retrieval," Neurocomputing **207**, 387–397 (2016).
9. M. T. Eismann and R. C. Hardie, "Stochastic spectral unmixing with enhanced endmember class separation," Appl. Opt. **43**, 6596–6608 (2004).
10. M. Xu, B. Du, and L. Zhang, "Spatial-spectral information based abundance-constrained endmember extraction methods," IEEE Trans. Geosci. Remote Sens. **7**, 2004–2015 (2014).
11. S. Gan, Q. Zhou, X. Xu, and Y. Hong, "Study on the surface roughness of substrate with multi-fractal spectrum," in *Proceedings of the 32nd International Conference on Micro- and Nano-Engineering* (2007), Vol. **84**, pp. 1806–1809.
12. M. Veganzones and M. Graña, "A spectral/spatial CBIR system for hyperspectral images," IEEE J. Sel. Top. Appl. Earth Obs. Remote Sens. **5**, 488–500 (2012).
13. R. Agrawal, H. Mannila, and R. S. Verkamo, "Fast discovery of association rules," in *Advances in Knowledge Discovery and Data Mining* (1996), Vol. **12**, pp. 307–328.
14. Q. K. Weinberger and K. S. Lawrence, "Distance metric learning for large margin nearest neighbor classification," J. Mach. Learn. Res. **10**, 207–244 (2009).
15. R. Kolpakov and K. Gregory, "Finding approximate repetitions under Hamming distance," Theoret. Comput. Sci. **303**, 135–156 (2003).

16. Z. Shao, W. Zhou, Q. Cheng, C. Diao, and L. Zhang, "An effective hyperspectral image retrieval method using integrated spectral," Sens. Rev. **35**, 274–281 (2015).
17. G. Salton and B. Chris, "Improving retrieval performance by relevance feedback," in *Readings in Information Retrieval* (1997), Vol. **24**, pp. 355–363.
18. Y. Zhang and D. Zhang, "Improved feature weight algorithm," Comput. Methods Appl. Mech. Eng. **37**, 210–213 (2011).
19. Q. Zhou, J. Zhang, Q. Tian, L. Zhuo, and W. Geng, "Automatic endmember extraction using pixel purity index for hyperspectral imagery," in *IEEE International Conference on Multimedia Modeling* (IEEE, 2016), pp. 207–217.
20. M. A. Shaban and O. Dikshit, "Improvement of classification in urban areas by the use of textural features: the case study of Lucknow city, Uttar Pradesh," J. Remote Sens. **22**, 565–593 (2001).
21. C. I. Chang and Q. Du, "Estimation of number of spectrally distinct signal sources in hyperspectral imagery," IEEE T. Geosci. Remote Sens. **42**, 608–619 (2004).
22. J. Hao and W. Zhang, "Image Euclidean distance based on kernel for face recognition," Comput. Eng. Des. **32**, 3844–3847 (2011).
23. N. Acito, G. Corsini, and M. Diani, "A novel technique for hyperspectral signal subspace estimation in target detection applications," in *IEEE International Geoscience and Remote Sensing Symposium* (IEEE, 2008), pp. 95–98.
24. J. Yu, "Texture image segmentation based on gaussian mixture models and gray level co-occurrence matrix," in *3rd International Symposium on Information Science and Engineering* (IEEE, 2010), pp. 149–152.
25. J. Zabalza, J. Ren, J. Ren, Z. Liu, and S. Marshall, "Structured covariance principal component analysis for real-time onsite feature extraction and dimensionality reduction in hyperspectral imaging," Appl. Opt. **53**, 4440–4449 (2014).
26. L. Grasso, "Synthetic advanced baseline imager true-color imagery," J. Appl. Remote Sens. **5**, 053520 (2011).
27. R. C. Gonzalez and R. E. Woods, *Digital Image Processing*, 3rd ed. (Prentice-Hall, 2008), p. 128.
28. H. Chen, T. Liang, and J. Yao, "The processing algorithms and EML modeling of true color synthesis for SPOT5 Image," Appl. Mech. Mater. **373**, 564–568 (2013).
29. W. Li and X. Lin, "Color composite of multi-spectral images based upon perceptive uniform color space," J. Opt. Technol. **1**, 9–13 (2007).
30. X. Fan, C. Fu, J. Shi, and L. Wu, "Remote sensing simulative truecolor fusion method based on principal components," J. Zhengzhou Inst. Surv. Mapp. **23**, 287–292 (2006).
31. M. Graña and M. Veganzones, "An endmember-based distance for content based hyperspectral image retrieval," Pattern Recognit. **45**, 3472–3489 (2012).